Large-Scale Colloidal Synthesis of Chalcogenides for Thermoelectric Applications

Viviana Sousa,^{1,2} Arka Sarkar,^{3,4} Oleg I. Lebedev,⁵ Christophe Candolfi,⁶ Bertrand Lenoir,⁶ Rodrigo Coelho,⁷ António P. Gonçalves,⁷ Eliana M. F. Vieira,^{8,9} Pedro Alpuim,^{1,2} Kirill Kovnir,^{3,4} and Yury V. Kolen'ko^{2,*}

¹Center of Physics of the Universities of Minho and Porto, University of Minho, Braga 4710-057, Portugal

²Nanochemistry Research Group, International Iberian Nanotechnology Laboratory, Braga 4715-330, Portugal

³Department of Chemistry, Iowa State University, Ames, Iowa 50011, United States

⁴Ames National Laboratory, U.S. Department of Energy, Ames, Iowa 50011, United States

⁵Laboratoire CRISMAT, UMR 6508, CNRS-ENSICAEN, Caen 14050, France

⁶Institut Jean Lamour, UMR 7198 CNRS-Université de Lorraine, 2 Allée André Guinier-Campus ARTEM, BP 50840, CEDEX, Nancy 54011, France

⁷Centro de Ciências e Tecnologias Nucleares (C2TN), Departamento de Engenharia e Ciências Nucleares, Instituto Superior Técnico, Universidade de Lisboa, Estrada Nacional 10, Bobadela LRS 2695-066, Portugal

⁸CMEMS – UMinho, University of Minho, Guimarães 4800-058, Portugal

⁹LABBELS – Associate Laboratory, Braga, Guimarães, Portugal

KEYWORDS: lead telluride; lead selenide; tin selenide; spark plasma sintering; microstructure; transport properties; Seebeck coefficient.

ABSTRACT. A simple and effective preparation of solution-processed chalcogenide thermoelectric materials is described. First, PbTe, PbSe, and SnSe were prepared by gram-scale colloidal synthesis relaying on the reaction between metal acetates and diphenyl dichalcogenides in hexadecylamine solvent. The resultant phase-pure chalcogenides consist of highly crystalline and defect free particles with distinct cube, rod, and tetrapod morphologies. The powdered PbTe, PbSe, and SnSe products were subjected to densification by spark plasma sintering (SPS), affording dense pellets of the respective chalcogenides. Scanning electron microscopy shows that the SPS-derived pellets exhibit fine nano/micro-structure dictated by the original morphology of the key constituting particles, while the powder X-ray diffraction and electron microscopy analyses confirm that the SPS-derived pellets are phase-pure materials, preserving the structure of the colloidal synthesis products. The resultant solution-processed PbTe, PbSe, and SnSe exhibit low thermal conductivity, which might be due to the enhanced phonon scattering over developed fine microstructure. For undoped n-type PbTe and p-type SnSe samples an expected moderate thermoelectric performance is achieved. In contrast, an outstanding figure-of-merit of 0.73 at 673 K was achieved for undoped *n*-type PbSe outperforming all majority of optimized PbSe-based thermoelectric materials. Overall, our findings facilitate the design of the efficient solutionprocessed chalcogenide thermoelectrics.

1. INTRODUCTION

Harvesting of waste heat is an interesting and sustainable approach for minimizing energy consumption. In particular, heat produced by electronic, mechanical, chemical, and nuclear systems, and even by human body could be recovered in form of electricity by means of solidstate thermoelectric (TE) devices. These devices perform the conversion of temperature gradients directly into electric voltages (Seebeck effect) and vice versa (Peltier effect). Notably, TE devices are mainly employed in niche markets, such as aerospace, military, vehicle waste heat recovery, consumer electronics, and internet of things.^{1,2} The efficiency of a TE device is determined by three factors, namely, thermal contacts, electrical interfaces, and the electric and thermal transport properties of constituent TE material. The TE material performance is measured by a dimensionless figure-of-merit, $ZT = \sigma S^2 T / \kappa$, wherein T is the absolute temperature, σ is the electrical conductivity, S is the Seebeck coefficient, and κ is the total thermal conductivity including an electronic, κ_e , and lattice, κ_L , parts. Although some state-of-the-art TE materials have recently reached ZT > 3, 3 common TE devices yet rely on Bi-based TE materials with $ZT \approx 1.2$ Increasing the TE efficiency of chalcogenides is of fundamental and long-standing interest given the role of the metal chalcogenides as a privileged class of industrially-relevant TEs. A particularly interesting solution for enhancing their ZT arises when micro/nano-structure is created within bulk material.⁴ Nanocrystals may tolerate larger number of atomic-scale defects (e.g., vacancies, dislocations) that act as phonon scattering centers, thus reducing the κ_L of the resultant chalcogenide TEs.⁵ Furthermore, construction of the chalcogenide TE materials from nano/microsized particles develops large number of grain boundaries, which effectively scatter phonons, thereby further reducing the κ_L of the resultant TE material.^{2,6,7} Solution-based syntheses have been widely applied to prepare nano/micro-sized chalcogenide particles for thermoelectric

application. The particles are further consolidated into bulk material via different sintering techniques, thus affording so-called solution-processed TEs with developed fine micro/nano-structure.

The highest $ZT \approx 2.05$ at 800 K has been reported for bulk PbTe–Ag₂Te composite material.⁸ An example of solution-processed PbTe was reported by Yang and co-workers,⁹ who synthesized n-type Bi-doped PbTe nanocubes by solvothermal method and thereafter, consolidated the nanocubes by spark plasma sintering (SPS). The resultant bulk PbTe material demonstrated a maximum $ZT \approx 1.35$ at 675 K owing to the combination of enhanced σ as a result of Bi doping and reduced κ due to the high density of grain boundaries and dislocations.⁹ Similar ZT = 1.2 at 620 K was reached by Fang and co-workers with PbTe–Bi₂Te₃ "barbell" nanowire heterostructures prepared by colloidal synthesis followed by consolidation via hot-pressing.¹⁰

With regard to solution-processed PbSe, p-type TE materials are typically obtained through wetchemistry followed by consolidation, while the most common approach to obtain rare n-type PbSe TEs includes post-synthesis treatments, such as ligand exchange. ^{11,12} For p-type PbSe, Zhou and co-workers reported a significant improvement in the TE performance of hydrothermally-derived nanostructured p-type PbSe through blending with Ag nanoparticles, attaining a maximum $ZT \approx 0.97$ at 723 K. ¹³ In another study, Cadavid and co-workers reached a $ZT \approx 0.6$ at 600 K for n-type PbSe colloidal nanoparticles having sodium amide ligands densified by hot-pressing. ¹² Nevertheless, best performance for bulk n-type PbSe-based TE material has been demonstrated by PbSe_{0.998}Br_{0.002}–2%Cu₂Se composite with a maximum $ZT \approx 1.8$ at 723 K, ¹⁴ indicating that further experimental exploration of n-type PbSe TEs is needed to reach higher ZT for the solution-processed materials.

SnSe has also found application as perspective TE material, with outstanding ZT = 3.1 at 783 K reported for bulk polycrystalline p-type SnSe material.³ Nanostructured solution-processed Gadoped SnSe synthesized by hydrothermal method followed by SPS densification was found to exhibit a maximum $ZT \approx 2.2$ and $ZT \approx 0.8$ at 873 K for doped and undoped SnSe, respectively.¹⁵ Nanocomposite SnSe–3%CdSe TE material prepared from nanoparticle building blocks showed a maximum $ZT \approx 2.2$ and $ZT \approx 1.35$ at 786 K for composite and pristine SnSe materials, respectively.¹⁶ In addition, doping with can afford interesting solution-processed TE materials, with maximum $ZT \approx 1.75$ at 873 K reached for 3 mol% Ge doping,¹⁷ $ZT \approx 1.7$ at 823 K for 2.3 atom% Cd doping,¹⁸ and $ZT \approx 1.05$ at 805 K for 2 atom% Te doping.¹⁹

Our laboratory has been exploring the colloidal syntheses^{20,21} of the chalcogenides in the context of their TE applications, wherein the as-synthesized low-dimension particles serve as building blocks for the preparation of either TE thin films with reduced thermal conductivity^{22–24} or bulk chalcogenides samples with enhanced ZT. Originally, we developed gram-scale colloidal synthesis of CuInSe₂ particles,²⁵ and then extended the scope of the developed synthesis protocol to the preparation of hexagonal-shaped plate-like Bi₂Te_{2.7}Se_{0.3} nanoparticles.²⁶ The nanoparticles were then subjected to SPS densification, which afforded nanostructured *n*-type Bi₂Te_{2.7}Se_{0.3} material exhibiting a maximum $ZT \approx 1$ at 373 K with an average $ZT \approx 0.93$ (300–473 K). More recently, we prepared composite (Bi,Sb)₂Te₃ nanoplatelets and Te-rich nanorods by the colloidal synthesis.²⁷ After SPS consolidation, the resultant Bi-based TE material exhibits a maximum $ZT \approx 1.4$ at 500 K. Considering the versatile synthetic potential of our colloidal synthesis towards chalcogenides, we were interested in expanding the scope of this synthesis beyond the preparation of nanostructured Bi-based TE materials. In particular, we explored the applicability of the

colloidal synthesis in combination with SPS consolidation for the preparation of undoped IV–VI chalcogenide TEs, namely, PbTe,²⁸ PbSe,²⁹ and SnSe.³

In this paper, we report gram-scale colloidal synthesis of highly-crystalline, undoped PbTe, PbSe, and SnSe particles with peculiar morphologies. Specifically, the end products were obtained through the reaction of metal (Pb or Sn) acetates with diphenyl dichalcogenides (Se or Te) in high-boiling hexadecylamine solvent. The as-synthesized particles were further consolidated into bulk pellets by means of SPS under optimized sintering conditions. Our TE properties characterization data indicates that a highly efficient nanostructured TEs can be obtained with this approach even for targeted undoped materials. For instance, our solution-processed n-type PbSe material exhibits a maximum figure-of-merit ZT = 0.73 at 673 K, indicating that the cost-effective colloidal synthesis in combination with SPS is a credible option for the fabrication of the efficient TEs.

2. EXPERIMENTAL SECTION

- **2.1. Reagents.** The following reagents were purchased and used as received: hexadecylamine (HDA, 95%, TCI), lead(II) acetate trihydrate (Pb(ac)₂·3H₂O, 99.99%, Sigma-Aldrich), tin(II) acetate (Sn(ac)₂, 99.9%, Sigma-Aldrich), diphenyl ditelluride (Ph₂Te₂, 98%, Sigma-Aldrich), diphenyl diselenide (Ph₂Se₂, 97%, TCI), absolute ethanol (99.8%, Honeywell), and toluene (99.8%, Fisher Scientific).
- **2.2. Synthesis.** To prepare PbTe, PbSe, and SnSe chalcogenides, our previously reported colloidal synthesis protocol was adapted,²⁵ which is schematically displayed in Figure 1. In a typical experiment, HDA (100 g, 414.1 mmol) and appropriate amounts of other reagents Pb(ac)₂·3H₂O (5.67 g, 14.9 mmol) and Ph₂Te₂ (3.97 g, 7.5 mmol) for PbTe synthesis; Pb(ac)₂·3H₂O (6.63 g, 17.5 mmol) and Ph₂Se₂ (4.09 g, 13.1 mmol) for PbSe synthesis; or Sn(ac)₂ (5.99 g, 25.3 mmol) and Ph₂Se₂ (5.92 g, 12.6 mmol) for SnSe synthesis were charged under ambient conditions into

a 500 mL round-bottom flask equipped with a magnetic stir bar, thermocouple, condenser, and vacuum adapter. The flask was then attached to a Schlenk line, and the mixture was slowly warmed to 90 °C while stirring accompanied by melting of HDA and homogenization of the reagents. The low boiling liquids, such as water and acetic acid admixtures, were removed by vacuum degassing of the reaction mixture at 90 °C for 1 h (SnSe synthesis) or for 2 h (PbTe and PbSe syntheses). An inert argon atmosphere was then introduced into the system, and the flask was rapidly heated up to 300 °C and stirred at this temperature for 1 h. Next, the heating source was removed, and the resultant greyish reaction mixture was naturally cooled to 80 °C and diluted with 80 mL of toluene while stirring. Afterward, the product was collected by centrifugation at 9000 rpm for 5 min, redispersed in toluene, and again collected by centrifugation at 9000 rpm for 5 min. The residual solid was then washed with a solvent mixture of toluene and ethanol (1:1) and collected by centrifugation at 9000 rpm for 5 min. After drying under vacuum, the product was finally homogenized with agate mortar and pestle to provide a fine powder. The yield of the assynthesized PbTe, PbSe, and SnSe was estimated to be around 90% (i.e., ca. 4.5 g of the end product).

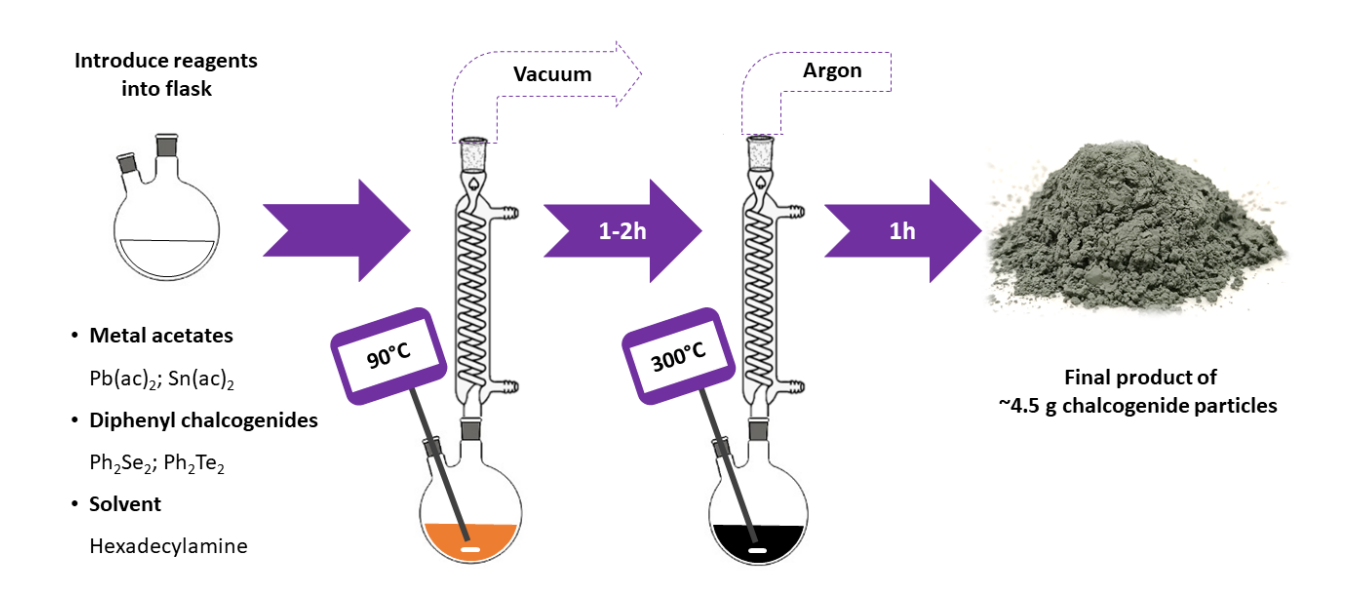


Figure 1. Schematic diagram of the colloidal synthesis protocol towards PbTe, PbSe, or SnSe chalcogenide particles.

2.3. Densification. To remove organic HDA ligands from the surface of the as-synthesized particles and to eliminate their possible surface oxidation, a heat treatment under flow of reductive atmosphere was carried out for the colloidal synthesis products prior to the SPS treatment. Accordingly, the samples were annealed under flow of H_2 : N_2 (1 : 4) at 350 °C for 3 h.

Pellets of PbTe, PbSe, and SnSe for TE property measurements were prepared by SPS using Dr. Sinter Lab Jr. SPS-211 Lx sintering unit (Kagaku). Finely ground synthesized chalcogenide powders were loaded into a 12.7 mm diameter graphite die with tungsten carbide plungers, and then sintered through the application of a uniaxial pressure P = 107 MPa and temperature T = 350 °C for t = 10 min. This temperature was chosen to avoid possible contaminations due to Se or Te evaporation. Next, excessive graphite from the SPSed samples was removed by polishing, and the resultant PbTe, PbSe, and SnSe pellets had densities of 99%, 96%, and 96% of their

theoretical crystallographic densities, respectively. These densities were determined by Archimedes-based method using toluene-displacement as the reference.

2.4. Characterization. The synthesized materials were analyzed by powder X-ray diffraction (XRD) using X'Pert PRO (PANanalytical) and Miniflex 600 (Rigaku) diffractometers employing Ni-filtered Cu K_{α} radiation. Scans were performed from 20–80° 2 θ while using Si-crystal zero-background sample holder. The XRD patterns were matched to International Centre for Diffraction Data (ICDD) PDF-4 database using HighScore software package (PANalytical). Pawley refinement was carried out using Topas 5.0 software package (Bruker).

The morphology and chemical composition of the synthesized particles and the SPSed materials were analyzed by scanning electron microscopy (SEM) using Quanta 650 FEG ESEM (FEI), fitted with an INCA 350 spectrometer (Oxford Instruments) for energy-dispersive X-ray spectroscopy (EDX). Particle sizes were estimated using ImageJ software package.

Fine microstructure and also chemical composition of the pristine and SPSed samples were investigated by high-angle annular dark-field scanning transmission electron microscopy (HAADF-STEM), electron diffraction (ED) and energy-dispersive X-ray spectroscopy in STEM mode (STEM-EDX) using a JEM-ARM200F microscope (Jeol), operated at 200 kV and equipped with cold field-emission gun, probe and image aberration correction, and a CENTURIO EDX detector.

The thermal behavior of the colloidal synthesis products was investigated by means of simultaneous thermogravimetric (TGA) and differential scanning calorimetry (DSC) analyses using STA 449F1 instrument (Netzsch). The powdered chalcogenides were heated from room temperature to 1000 °C at 10 °C min⁻¹ under a continuous argon flow of 50 mL min⁻¹.

The Seebeck coefficient, S, and thermal conductivity, κ , were measured using a Nemesis SBA 458 tool (Netzsch), equipped with a four-probe option. Thermal diffusivity of the samples was measured using a LFA 467 system by the laser flash method (Netzsch). The thermal conductivity values were calculated by means of multiplying measured thermal diffusivity values by the corresponding densities and specific heat capacities of each SPSed sample. Electronic thermal conductivity (κ e) was calculated using the Wiedemann-Franz law, κ e = $L \times \sigma \times T$ (where L = Seebeck coefficient dependent Lorenz number in 10^{-8} W Ω K⁻²; σ = electrical conductivity in S m⁻¹; T= temperature in Kelvin). The Seebeck coefficient dependent L was calculated using the following equation: L = 1.5 + exp [-|S|/116]; where L is in 10^{-8} W Ω K⁻² and S is in μ V K⁻¹. Lattice thermal conductivity (κ L) was calculated by κ L = $\kappa - \kappa$ e.³⁰

Hall measurements were made PbSe rectangular dimensions on bar with $\approx 1.38 \times 4.44 \times 6.82 \text{ mm}^3$, that was cut from the SPSed PbSe pellet. The measurements were carried out using the Electrical Transport Option on Physical Properties Measurement System (Quantum Design) with a 5-probe set up (Figure S1) using a constant current $I_x = 0.1$ mA within a range of magnetic field (B_z) between -3 T to 3 T, acting perpendicular to the rectangular bar. The measurements were repeated at different temperatures, namely, 5, 75, 150, 225, 300 and 375 K, to observe the temperature-dependence of the Hall coefficient $(R_{\rm H})$, carrier concentration (n) and Hall mobility (μ) of the SPSed PbSe. The voltage measured across Channel 2 (Figure S1) is the Hall voltage (V_H). R_H was calculated by $R_H = (V_H \times t) / (I_X \times B_z)$; where t = thickness of the bar (1.38 mm). Carrier concentration (n) was calculated using the following equation: $n = 1 / (|R_{\rm H} \times e|)$; where e = electronic charge. Hall mobility (μ) was calculated using $\mu = (R_{\rm H} / \rho)$; where ρ = resistivity of the material measured along Channel 1 (Figure S1) at B_z = 0 T at any specific temperature. R_H , n and μ were then plotted as a function of the corresponding temperature values.³¹

3. RESULTS

3.1. Phase-pure chalcogenide particles with peculiar morphology. Our previously reported colloidal synthesis method used to prepare CuInSe2²⁵ served herein as the base for the synthesis of PbTe, PbSe, and SnSe chalcogenides. Reacting metal acetates with diphenyl dichalcogenides in fatty hexadecylamine solvent followed by product isolation and purification reproducibly afforded the solids with an excellent yield of about 90%. An attractive feature of this synthesis protocol is that it gives access to large quantities (ca. 4.5 g) of the target compounds, thus providing enough materials for further characterization and processing. According to the XRD analysis, the end products of the colloidal synthesis were identified as phase-pure cubic PbTe (Figure 2a, ICDD no. 04-016-1608), cubic PbSe (Figure 2b, ICDD no. 04-003-4844), as well as orthorhombic SnSe (Figure 2c, ICDD no. 01-081-9463). The refined cell parameters of the as synthesized materials are in close agreement with literature values. In addition, elemental analysis by EDX spectroscopy also confirmed that the as-synthesized samples are phase-pure materials (Figures S2a,c,e).

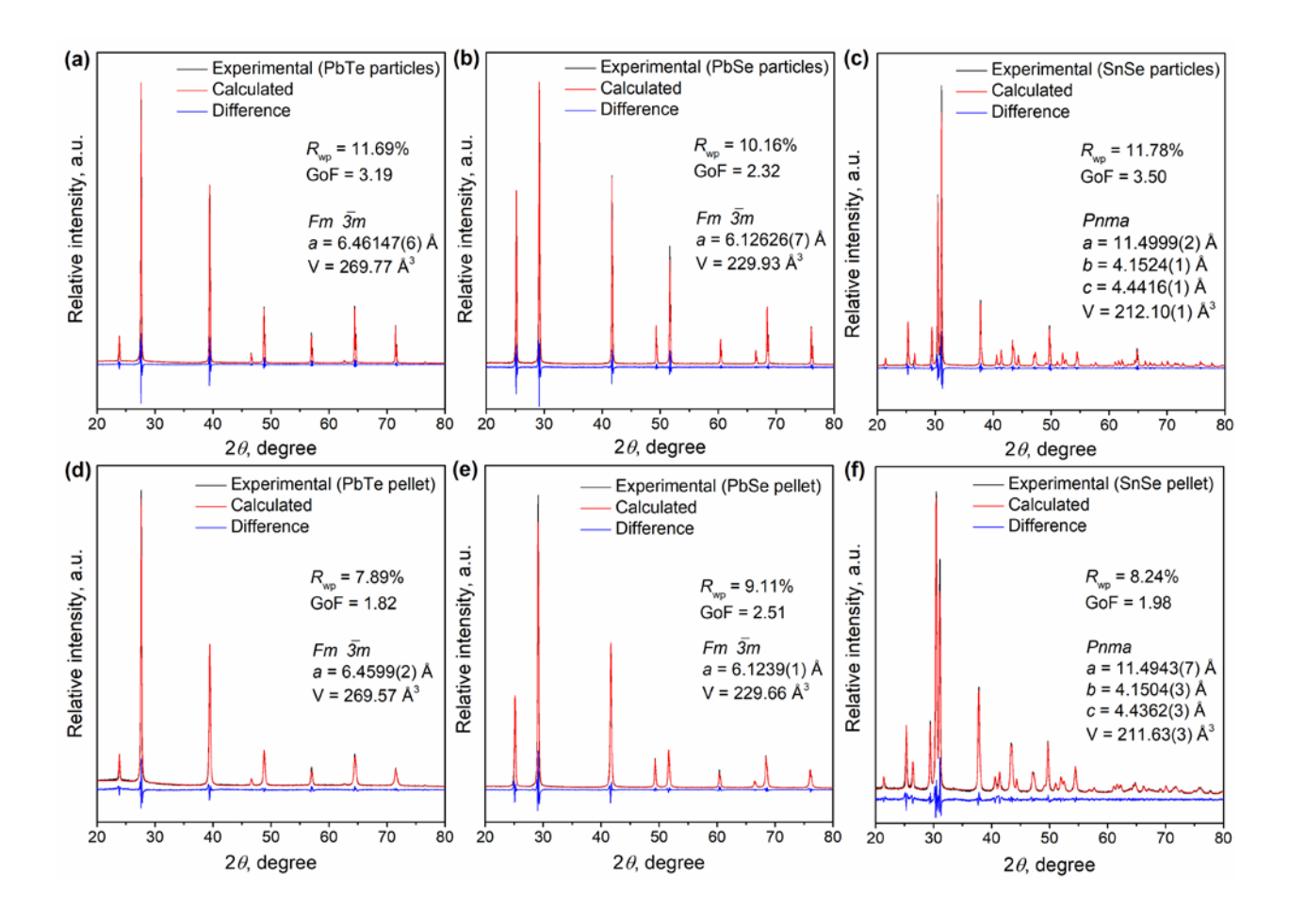


Figure 2. Collected XRD patterns (black), calculated pattern based on crystal structure (red) and Pawley refinement (blue) for the synthesized colloidal products (top panel) and the respective SPSed pellets (bottom panel) for PbTe (a,d), PbSe (b,e), and SnSe (c,f). Pawley refinement was performed and resulting values of R_{wp} , goodness of fit (GoF), and refined lattice parameters are provided.

To investigate the morphological features of the PbTe, PbSe, and SnSe synthesized by the colloidal method, SEM analysis was carried out. The observation of the PbTe product reveals that this product consists of faceted particles exhibiting a nonuniform size distribution ranging from 200 nm to 4 µm (Figures 3a, S3a,b). Many of these particles appear to possess a fairly concave cubic shape. PbSe particles were observed to be similar in size to PbTe ones while possessing a nonuniform

size distribution as well ranging from 500 nm to 3 μm and featuring tetrapod-like appearance (Figures 3b, S3c,d). In contrast, the SnSe product consists of elongated rod-like particles (Figures 3c, S3e,f). Compared to PbTe and PbSe, SnSe crystals are considerably larger in size with a nonuniform distribution (2–40 μm).

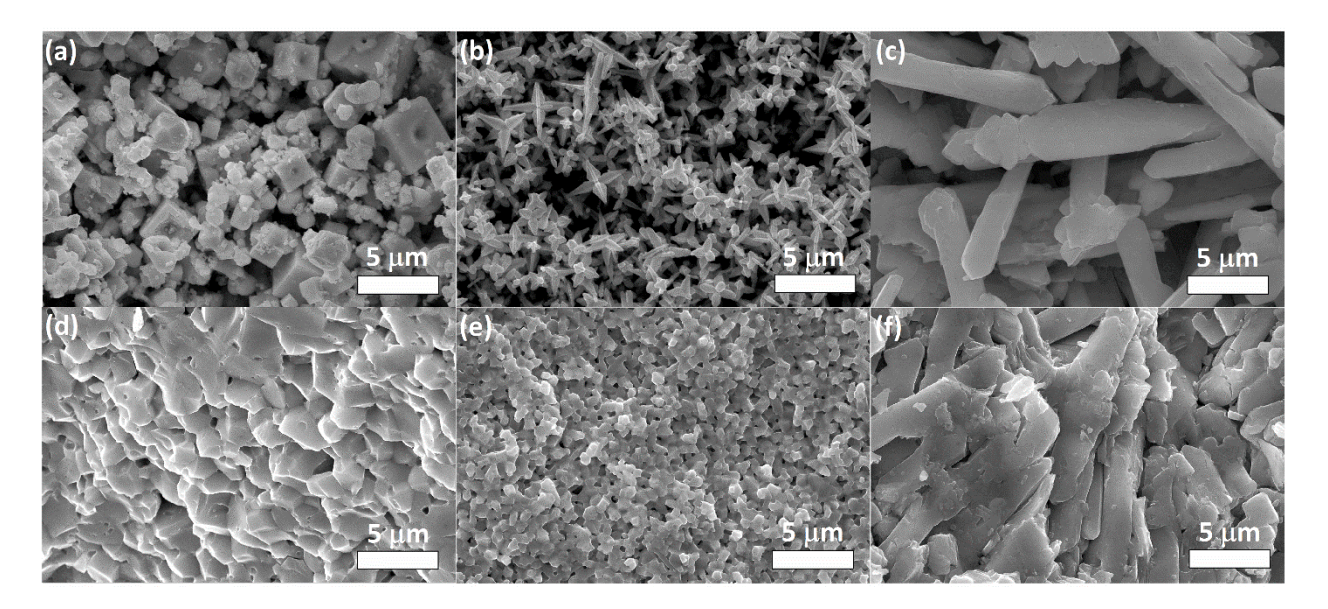


Figure 3. Representative SEM images of the synthetized colloidal products (a,b,c) and the respective SPSed pellets (d,e,f) of PbTe (a,d), PbSe (b,e), and SnSe (c,f).

We have further studied fine microstructure and chemical composition of the colloidal synthesis products by electron microscopy techniques, and the results for each of the SnSe, PbSe, and PbTe samples are given in Figures 4–6, respectively. Collected along main zone axis, ED patterns and the representative high-resolution HAADF–STEM images confirmed the crystal structure determined from XRD – cubic (Fm–3m, a = 6.46 Å) for PbTe (Figure 4), cubic (Fm–3m, a = 6.13 Å) for PbSe (Figure 5), as well as orthorhombic (Pnma, a = 11.5 Å, b = 4.15 Å, c = 4.44 Å) for SnSe (Figure 6). All images evidence an overall high crystallinity and defects-free structure of the synthesized PbTe, PbSe, and SnSe particles (Figures 4–6). The performed image simulations for PbSe (Figure 5) and SnSe (Figure 6) show excellent agreements with an

experimental HAADF–STEM images. No point defects have been observed. Since the PbTe and PbSe are isostructural with slightly different *a* parameter, the HAADF–STEM images, as expected, are similar (Figures 4,5), and hence, the image simulation for PbTe (Figure 4) was not performed. Elemental STEM–EDX maps highlight the homogeneous distribution of the key constituent elements inside the synthesized particles, confirming that the particles are pure PbTe (Figure S4), PbSe (Figure S5), and SnSe (Figure S6), devoid of any secondary phases.

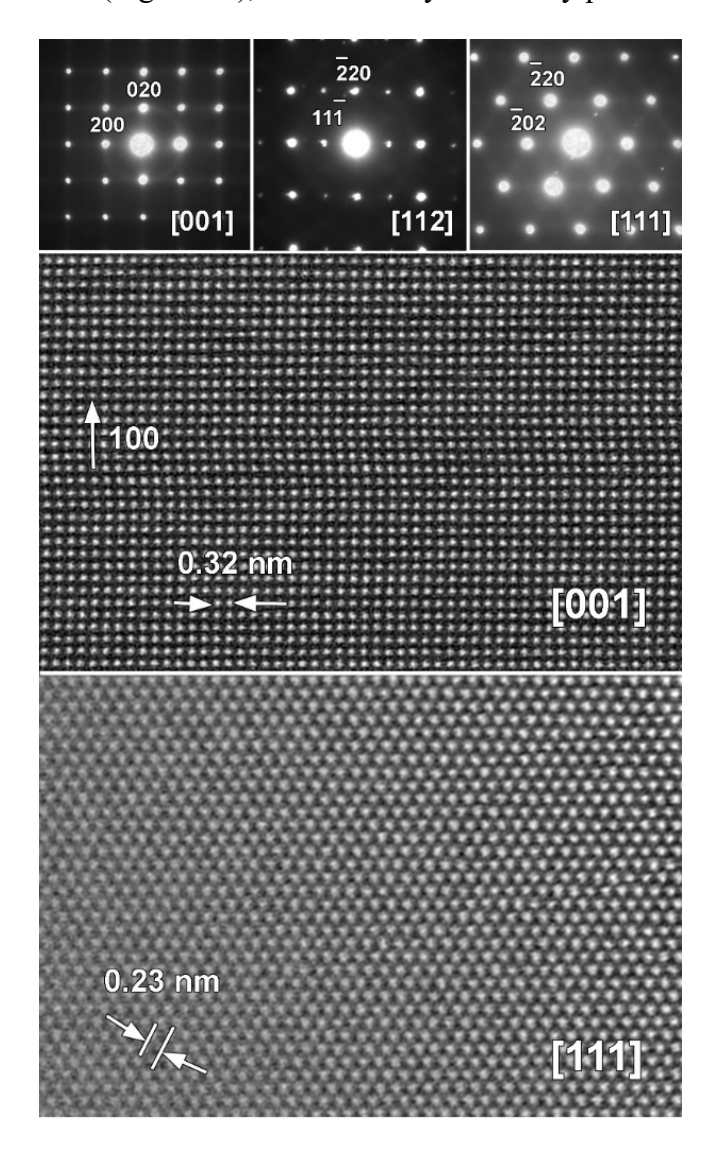


Figure 4. ED patterns collected along main zone axes of PbTe particles synthesized by the colloidal method, together with the corresponding high-resolution [001] and [111] HAADF–STEM images.

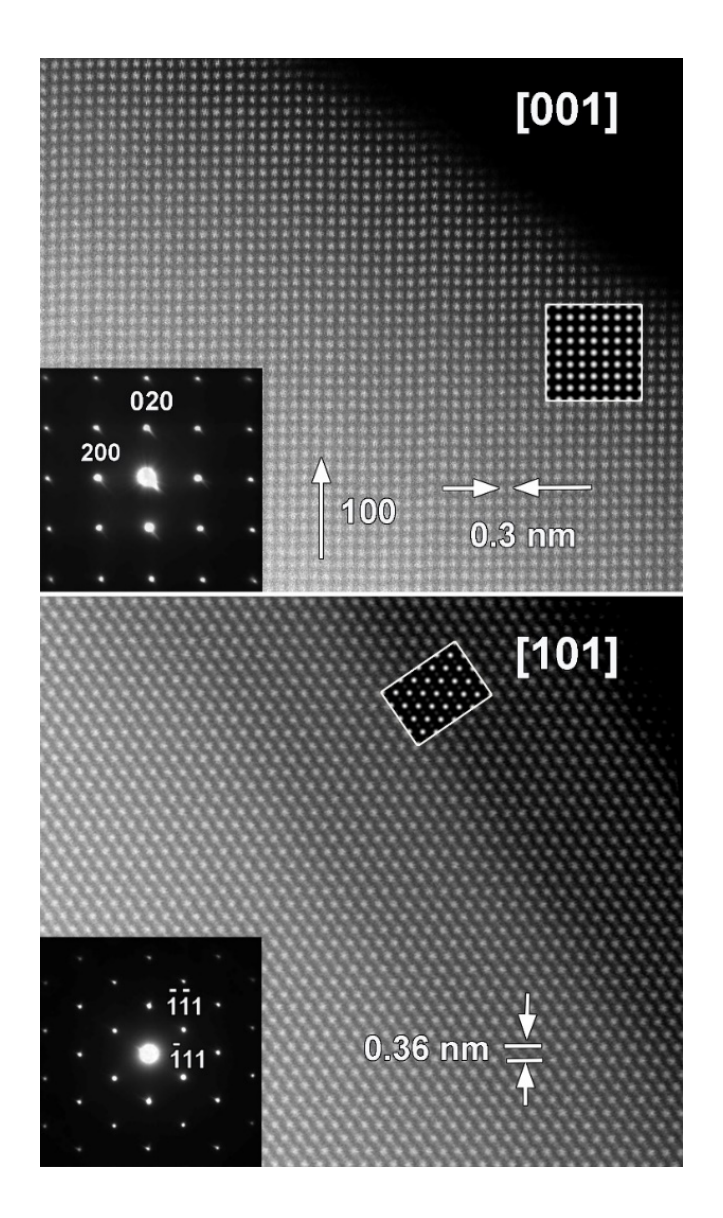


Figure 5. High-resolution HAADF–STEM images and the corresponding ED patterns along main [001] and [101] zone axes of cubic Fm–3m structure of PbSe synthesized by the colloidal method. Simulated images based on cubic Fm–3m structure are given as insert.

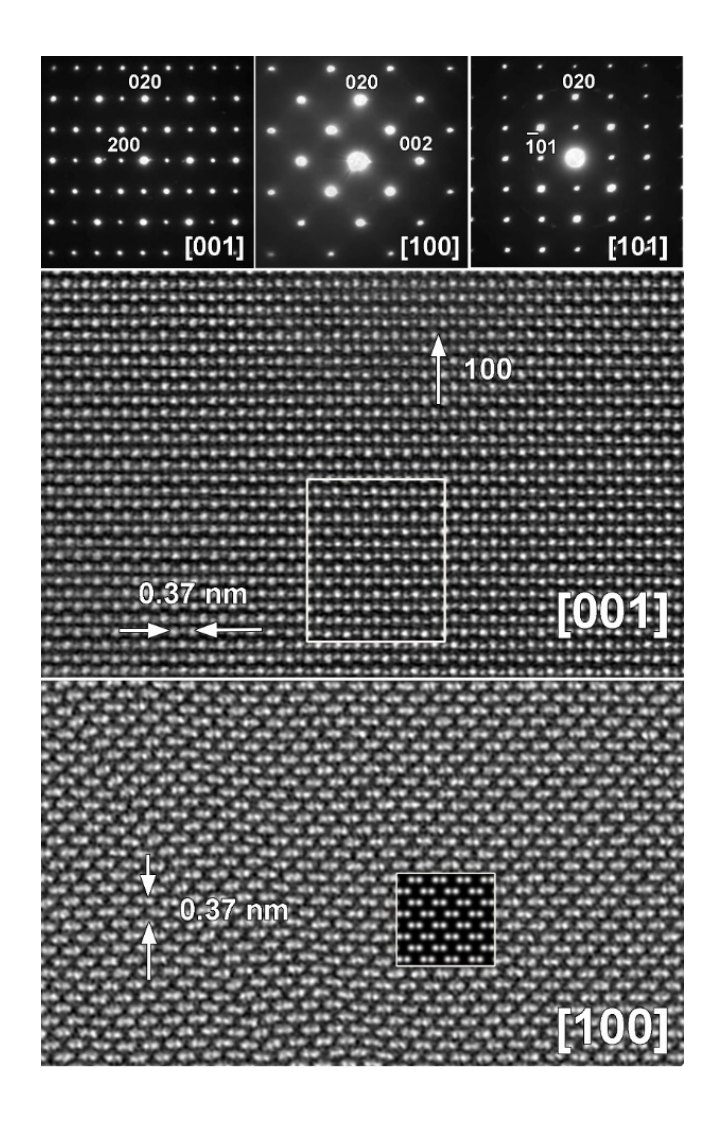


Figure 6. ED patterns collected along main zone axes for SnSe particles synthesized by the colloidal method, together with the corresponding high-resolution HAADF–STEM images taken along [001] and [100] zone axes. Simulated images based on orthorhombic *Pnma* structure are given as insert.

For the high temperature TE applications, the thermal stability of the as synthesized materials was characterized by means of TGA/DSC analyses. The results show that PbTe (Figure S7) and SnSe (Figure S8) chalcogenides have an excellent thermal stability up to 700 °C, while PbSe (Figure S9) exhibits even higher stability up to 850 °C. Only above these high temperatures and till maximum

studied temperature of 1000 °C, the samples undergo the total weight losses of 4%, 18%, and 53% for PbTe, PbSe, and SnSe, respectively (Figures S7–S9).

3.2. Phase-pure densified chalcogenide pellets with developed microstructure. In the current study, the µm-sized PbTe, PbSe, and SnSe products of the colloidal syntheses were consolidated into the respective TE materials by means of SPS. This process results in the formation of bulky PbTe, PbSe, and SnSe pellets with densities of 99%, 96%, and 96%, respectively, of their theoretical crystallographic densities. According to the XRD analysis, the SPS processing preserves the phase structure of the initial chalcogenides synthesized by colloidal method, since neither secondary phases nor significant structural changes were detected by XRD characterization (Figure 2). Refinements of the unit cell parameters (Figure 2) indicated that small shrinking in the unit cell parameters have occurred after SPS, which might be caused by the annealing of the defects during the sintering.

Chemical analysis of the SPSed pellets by EDX spectroscopy further indicates their phase purity (Figures S2b,d,f), confirming that chemical composition of the pristine chalcogenide particles remains essentially unchanged after SPS consolidation at P = 107 MPa, T = 350 °C, and t = 10 min. To evaluate the microstructure of the resultant SPSed pellets, SEM observations were performed. All densified chalcogenides demonstrate compact microstructure, as shown in Figures 3d,e,f and S10a,b,c. The characteristic morphologies (cube- and rod-like) of the initial chalcogenide particles are still visible after SPS consolidation (Figures 3a,b,c *cf.* Figures 3d,e,f). This finding suggests that the initial chalcogenide particles did not melt during SPS but rather sinter together, which results in the structural solidity of the SPSed PbTe, PbSe, and SnSe materials. The electron microscopy investigation of the SPSed samples further indicates that the

sintering affords highly crystalline, defect-free, chemically uniform, and phase-pure materials (Figures S11–13).

3.3 Transport properties and thermoelectric performance. After consolidating the synthesized PbTe, PbSe, and SnSe particulate products by SPS into high-density sintered pellets, their temperature-dependent thermoelectric properties were characterized in a temperature range of 298–673 K (Figures 7,8). Maximizing figure-of-merit requires materials with low thermal conductivity, high electrical conductivity, and a large Seebeck coefficient.

Several phonon scattering approaches may reduce lattice thermal conductivity, including micro/nano-structuring, alloying, and anharmonic lattice vibrations. Nanostructuring increases boundary scattering, alloying introduces point defect scattering, while anharmonic lattice vibrations enable a strong inherent phonon-phonon scattering.³² Thermal conductivity for all samples reported here is quite low (Figure 7), as expected from their fine microstructure (Figures 3d,e,f and S10a,b,c) that increases phonon scattering.³³ The total thermal conductivity, κ , for all samples decreases with increasing the temperature (Figure 7a). For PbTe, κ reached a minimum value of 1.1 W m⁻¹ K⁻¹, while for PbSe and SnSe, κ was even lower with 0.9 and 0.3 W m⁻¹ K⁻¹, respectively, at 623 K.

Lattice thermal conductivity, κ_L , and electronic thermal conductivity, κ_e , were also calculated (Figures 7b,c). Notably, κ_e values of the SPSed PbTe and SnSe chalcogenides (Figure 7c) were found to have negligible contribution to total κ because of the low electrical conductivity of these materials, whereas κ_e of highly conductive SPSed PbSe has a significant contribution to total κ . SnSe and PbTe samples exhibit relatively low values of electrical conductivity, reaching $\sigma = 0.9 \times 10^3 \text{ S m}^{-1}$ at 623 K and $\sigma = 6.4 \times 10^3 \text{ S m}^{-1}$ at 673 K, respectively (Figure 8a). In contrast, PbSe exhibits excellent temperature-dependent values of σ with a maximum of

 $6.4 \times 10^4 \, \mathrm{S \ m^{-1}}$ near RT (Figure 8a). In contrast to PbTe and SnSe, σ of PbSe is decreasing with temperature.

Lattice thermal conductivity of bulk PbTe is *κ*_L ≈2 W m⁻¹ K⁻¹ at room temperature (RT).²⁸ Our micro/nano-structured PbTe shows a comparable $\kappa_L \approx 1.9 \text{ W m}^{-1} \text{ K}^{-1}$ at RT, which decreases to $\kappa_L \approx 1~W~m^{-1}~K^{-1}$ at 672 K (Figure 7b). Introduction of point defects and dislocations was shown to decrease κ_L to 0.8 W m⁻¹ K⁻¹ for PbTe–PbS alloys, whereas the formation of Pb precipitates in InSb-doped PbTe resulted in an even more reduced $\kappa_L \approx 0.3 \text{ W m}^{-1} \text{ K}^{-1}$, which is lower than the amorphous limit $\kappa_L \approx 0.32~W~m^{-1}~K^{-1}$ for PbTe.³⁴ In the SPSed PbSe, lattice thermal conductivity decreases from $\kappa_L \approx 1.4 \text{ W m}^{-1} \text{ K}^{-1}$ at RT to $\kappa_L \approx 0.7 \text{ W m}^{-1} \text{ K}^{-1}$ at 673 K (Figure 7b), with both values slightly lower than $\kappa_L \approx 1.3 \text{ W m}^{-1} \text{ K}^{-1}$ near RT and $\kappa_L \approx 0.8 \text{ W m}^{-1} \text{ K}^{-1}$ at 700 K measured for bulk PbSe. 13,29 Zhou and co-workers obtained lower k for PbSe system through the incorporation of Cu and Te nanostructures into bulk PbSe material, reaching $\kappa_L \approx 0.2 \text{ W m}^{-1} \text{ K}^{-1}$ at 773 K, 35 which is lower than the amorphous limit $\kappa_L \approx 0.40 \text{ W m}^{-1} \text{ K}^{-1}$ for PbSe. 34 The estimated κ_L for the SPSed SnSe changes from $\kappa_L \approx 0.7~W~m^{-1}~K^{-1}$ at RT to $\kappa_{latt} \approx 0.3~W~m^{-1}~K^{-1}$ at 623 K (Figure 7b), consistent with the calculated $\kappa_L \approx 0.7 \text{ W m}^{-1} \text{ K}^{-1}$ at 300 K for Sn_{1-x}Se , ³⁶ as well as the reported κ_L values in other SPSed SnSe nanoparticles. ¹⁹ Notably, by tuning chemical composition of SnSe, vacancies (V_{Sn} or V_{Se}) were introduced that significantly reduced κ_{L} when compared with SnSe without vacancies ($\kappa_L \approx 1.4~\mathrm{W~m^{-1}~K^{-1}}$ at 300 K). ³⁶ Further compositional tuning of SnSe and elimination of persistent SnO_x compound enabled κ_L values as low as 0.07 W m⁻¹ K⁻¹ at 783 K for polycrystalline SnSe.³

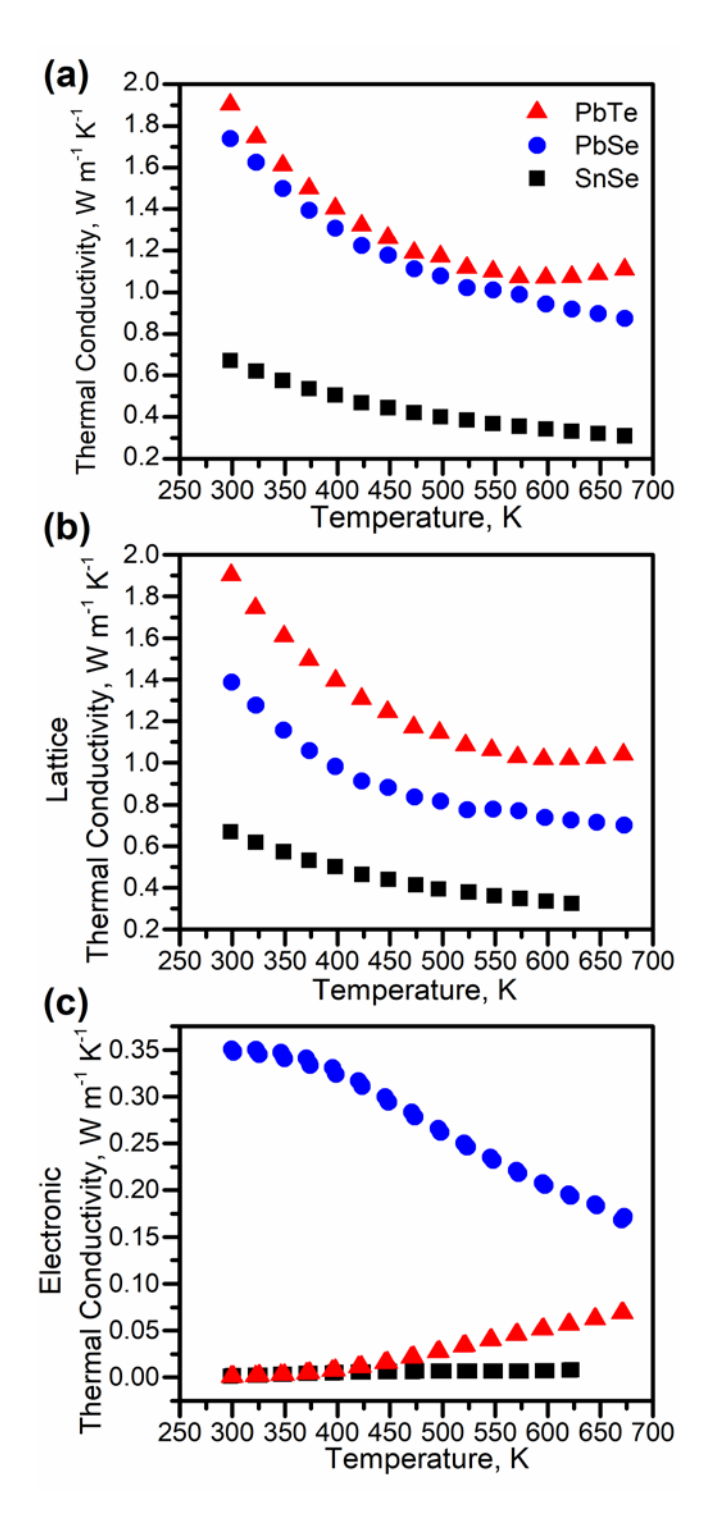


Figure 7. Total (a), lattice (b), and electronic (c) thermal conductivities of the SPSed PbTe, PbSe, and SnSe materials.

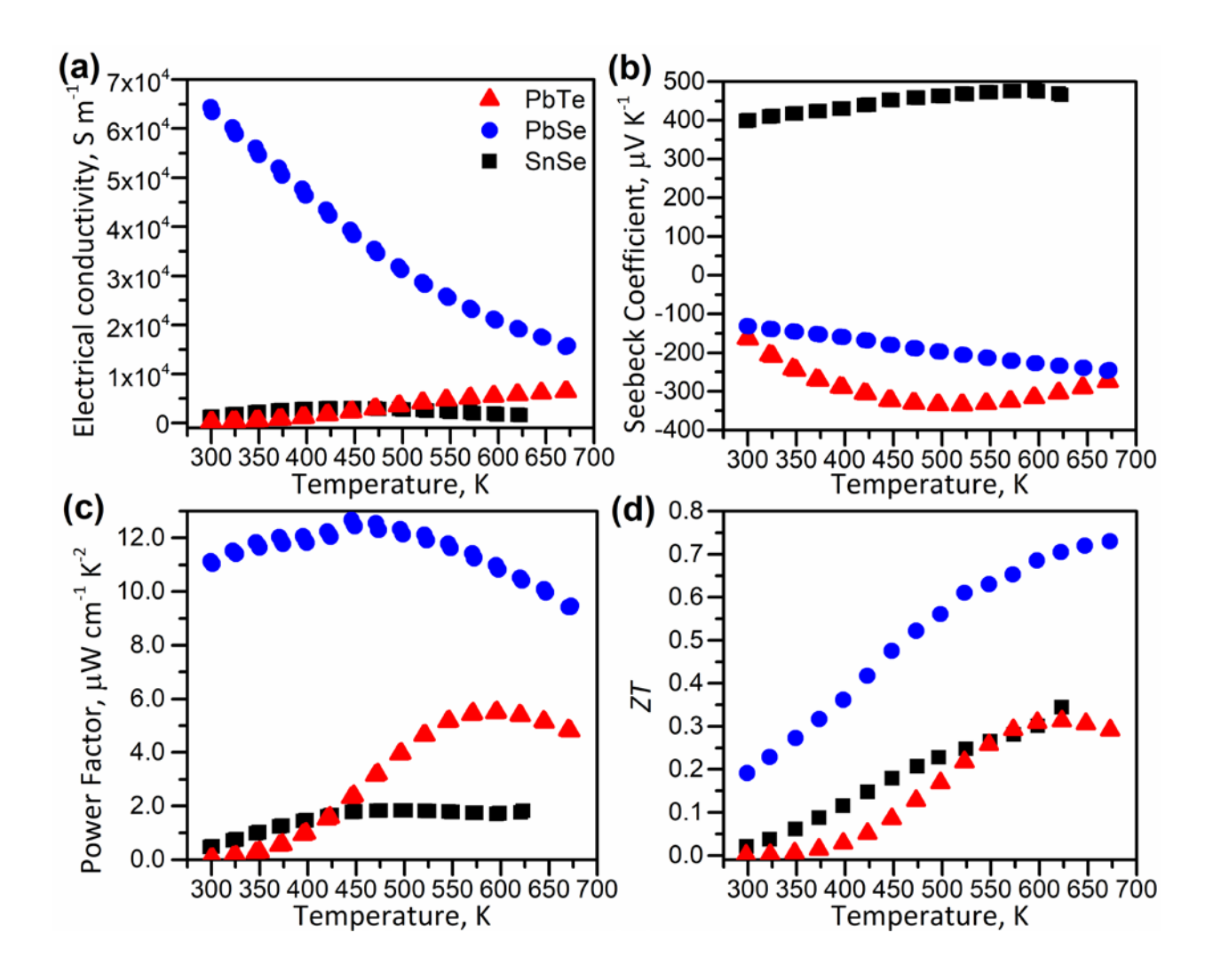


Figure 8. Temperature-dependent electrical conductivity (a), Seebeck coefficient (b), power factor (c), as well as figure-of-merit (d) of the PbTe, PbSe, and SnSe materials obtained by SPS densification of the respective colloidal synthesis products.

The observed positive Seebeck coefficient, S, for SnSe reveals that this SPSed material is p-type with holes as main charge carriers, while the negative values measured for PbTe and PbSe indicate that these materials are n-type having electrons as main charge carriers (Figure 8b). Maximum S values were estimated to be $S = -334 \,\mu\text{V K}^{-1}$ at 521 K for PbTe, $-S = 247 \,\mu\text{V K}^{-1}$ at 670 K for PbSe, and $S = 476 \,\mu\text{V K}^{-1}$ at 596 K for SnSe (Figure 8b). Since both PbTe and SnSe products reached the maximum Seebeck coefficient before the highest measured temperature, we can

estimate their bandgap following the Goldsmid-Sharp formalism as $E_g = 2e|S_{max}|T_{max}$, where e is the elementary charge, S_{max} is the maximum Seebeck coefficient value reached, and T_{max} is the absolute temperature at which S_{max} occurs.³⁷ The bandgap value calculated for SPSed PbTe ($E_g = 0.27 \text{ eV}$) is quite close to the value of bulk PbTe ($E_g \approx 0.3 \text{ eV}$),³⁸ while calculated value for SnSe ($E_g = 0.44 \text{ eV}$) appeared to be lower than the value of $E_g = 0.86 \text{ eV}$ for bulk SnSe.³⁹ The bandgap for PbSe was not calculated since S_{max} was not reached in the measured temperature range (Figure 8b).

Power factors (*PF*) were calculated for all the three SPSed materials (Figure 8c), where PbTe had an increase in *PF* at elevated temperatures, peaking $PF = 6 \mu \text{W cm}^{-1} \text{ K}^{-2}$ at 600 K. At the same time, PbSe recorded remarkable *PF* throughout the entire temperature range, reaching a peak $PF = 13 \mu \text{W cm}^{-1} \text{ K}^{-2}$ at 445 K. This is about half of the exceptionally high *PF* value for recently reported Cu/Te co-doped PbSe material with a peak *ZT* value of 1.3.³⁵

Hall measurements carried out on the SPSed PbSe sample within a range of 5 K to 375 K (Figure 9) showed lower carrier concentration values $4-5 \times 10^{18}$ cm⁻³ (Figure 9a) when compared to most reported PbSe-based TE materials, which explains the high *S* values observed throughout the entire temperature range (Figure 8b).⁴⁰ Hall mobility reaches a peak value of 290 cm² V⁻¹ s⁻¹ at 150 K before it starts decreasing with the temperature (Figure 9b). Such high values of carrier mobility in the SPSed PbSe justify its high σ , as well as its high κ e contribution to total κ (Figures 7a,c), as opposed to that for SnSe and PbTe exhibiting low κ e (Figure 7c). High carrier mobility also confirms defect-free nature of this material, consistent with the electron microscopy results (Figure S12), thus suggesting that our large-scale synthesis could be used as an optimized way of producing defect-free PbSe-based materials in future research.⁴⁰

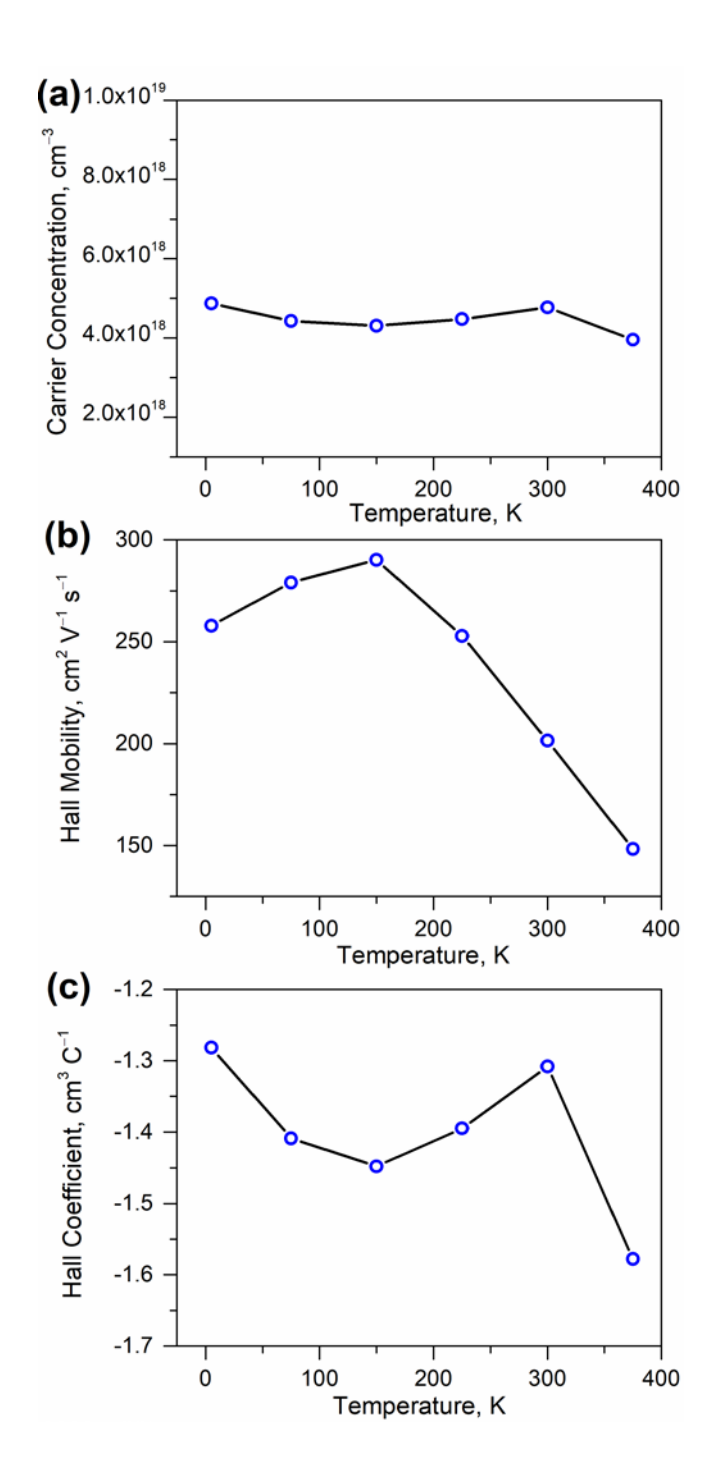


Figure 9. Carrier concentration (a), Hall mobility (b), and Hall coefficient (c) for the SPSed PbSe.

Overall, with simultaneous high σ , high S and reduced κ , n-type PbSe as reported here, exhibits the topmost TE performance with a maximum ZT = 0.73 at 673 K (Figure 8d). In comparison, recent reports suggested a carrier concentration of 3×10^{18} cm⁻³ and an exceptional carrier

mobility of 1229 cm² V⁻¹ s⁻¹ at RT for undoped polycrystalline PbSe, albeit with a much higher thermal conductivity compared to ours, resulting in a slightly lower peak $ZT \approx 0.6$ at 400 K.⁴¹ Some other comparable PbSe-based materials include Mo-doped PbSe with a comparable carrier concentration value of $5 \times 10^{18} \, \mathrm{cm}^{-3}$ with an exceptional $PF = 33 \, \mu \mathrm{W \ cm}^{-1} \, \mathrm{K}^{-2}$ at room temperature. 42 However, one of the best performing materials is Cr-doped PbSe with an extremely high carrier mobility of $1100~\text{cm}^2~\text{V}^{-1}~\text{s}^{-1}$ and a low carrier concentration of $1\times10^{18}~\text{cm}^{-3}$ at room temperature, leading to a high room temperature $PF = 30 \mu \text{W cm}^{-1} \text{ K}^{-2}$ and a peak $ZT \approx 1.0$ at elevated temperature. 42 It suggests that our undoped PbSe has a peak performance close to one of the best reported doped PbSe-based materials. With negative Hall (R_H) (Figure 9c) and Seebeck coefficients values (Figure 8b) in our PbSe material signifying n-type conduction, it can be hypothesized that successful hole-doping via our experimental method can lead to a further reduction of carrier concentration and an increased PF, resulting in an improvement in its thermoelectric performance, with potential of reaching the performances of the best reported PbSebased TE materials, such as Sb-doped PbSe and Na-doped PbSe. 41-47 Besides the exceptional performance observed for undoped PbSe, lower maximum ZT values of 0.31 and 0.34 at 623 K (Figure 8d) were estimated for our undoped PbTe and SnSe, respectively, mainly as a result of their low σ (Figure 8a).

4. DISCUSSION

Merging wet-chemistry-based synthesis methods of TE nanomaterials (*e.g.*, colloidal, hydrothermal, solvothermal, precipitation)⁴⁸ with their subsequent consolidation into bulky solids (*e.g.*, by SPS or hot-pressing) opens facile, cost-effective, and scalable preparation access to a diversity of nano/micro-structured TEs with improved performance. Notably, the synthesis method should be easily scalable to provide enough material for the fabrication of the functional TEs. This

study illustrates how a set of undoped chalcogenide compounds could be prepared in high yield at large-scale. In the classic hot-injection colloidal synthesis, one could obtain colloidal chalcogenide nanoparticles with narrow size and shape distributions, albeit usually in low quantities on milligram scale.^{20,21} On the other hand, our versatile heating-up colloidal synthesis allows to obtain multigram of highly crystalline and defect free chalcogenide particles with an interesting morphologies just in one run, highlighting the applicability of the synthesis for upscaled production of chalcogenide-based TE materials.

Interestingly, the chalcogenide particles synthetized in the current study by heating-up colloidal synthesis demonstrate peculiar morphological appearances, namely, cubic-, tetrapod- and rod-like shapes for PbTe, PbSe, and SnSe, respectively. Previously published experimental work9 shows that PbTe with similar cubic-like morphology can be obtained by solvothermal synthesis, but with significantly smaller size 100–150 nm compared to our PbTe product (Figures 3a, S3a,b). Regarding the morphology reported for PbSe, sea-urchin-like appearance with 500–600 nm in size was observed for hydrothermally-synthesized product, 13 while our colloidal synthesis method provides access to tetrapod-like shape with few micrometers in size (Figures 3b, S3c,d). Reported SnSe particles exhibit several morphologies: (i) square-like nanoplates with size of 4 µm were synthesized by hot-injection colloidal method, ¹⁹ (ii) smaller nanoplates with irregular shapes were synthesized by hydrothermal route, ^{15–17} and (*iii*) 120 µm-sized flower-like particles were produced by solvothermal synthesis. 18 In contrast, SnSe synthesized in the current study demonstrates rodlike appearance with few tens of micrometers in size (Figures 3c, S3e,f). The diversity of peculiar but sometimes uncommon morphologies obtained for our PbTe, PbSe, and SnSe products affords an interesting possibility to control the microstructure of the derivative TE materials after consolidation, like demonstrated herein (Figures 3a,b,c and S3 cf. Figure 3d,e,f and S10).

Our large-scale synthesis route was further leveraged to fabricate and investigate bulk pellets of PbTe, PbSe, and SnSe TEs. Figure 10 compares the TE performance of the derived materials with other solution-processed chalcogenide TEs (*i.e.*, synthesis of the material by wet chemistry followed by densification) reported in the literature. Our *n*-type PbTe shows significantly lower maximum ZT = 0.31 (623 K) compared to the reported solution-processed PbTe with maximum ZT = 1.2 (623 K).^{9,10} A likely explanation is the low electrical conductivity of our SPSed PbTe (Figure 8a), but the TE efficiency of the PbTe could be improved through tailoring SPS densification conditions (P, T, t) combined with material's chemical composition tuning (doping, compositing).² Given the best bulk PbTe–Ag₂Te composite TE material has $ZT \approx 1.5$ (623 K),⁸ these are interesting experimental research directions for optimization of our n-type PbTe material.

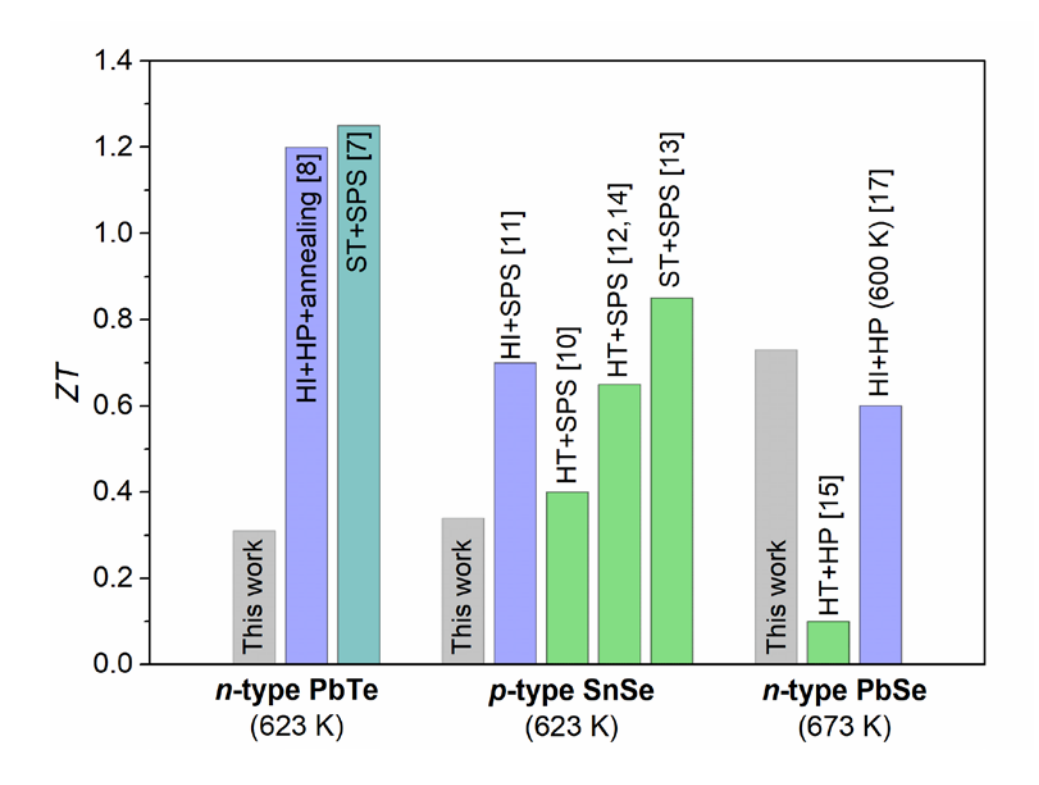


Figure 10. Comparison of figure-of-merit ZT values for the various solution-processed n-type PbTe and PbSe as well as p-type SnSe. Abbreviations are associated with the applied wet chemistry

route (HI: hot-injection, ST: solvothermal, HT: hydrothermal) and densification method (HP: hot-press, SPS: spark plasma sintering).

An excellent ZT = 2.1 at 623 K has been reported for bulk polycrystalline p-type SnSe material.³ At the same time, lower ZT values were reported (ZT = 0.24–0.45) for solution-processed undoped SnSe TEs, ^{15,17,19} while higher $ZT \approx 0.65$ –0.85 values have been reported for solution-processed SnSe doped by Ga, CdSe, or Cd (Figure 10). ^{15,16,18} We obtained a comparable ZT = 0.34 at 623 K for our solution-processed undoped SnSe material, which is predominantly due to its low electrical conductivity (Figure 8a). Noteworthy are the remarkably low thermal conductivities of our SPSed SnSe ($\kappa = 0.67$ W m⁻¹ K⁻¹ at 300 K and $\kappa = 0.31$ W m⁻¹ K⁻¹ at 673 K), which is comparable with some of the lowest values reported for high-performing bulk SnSe ($\kappa = 0.65$ W m⁻¹ K⁻¹ at 300 K and $\kappa = 0.23$ W m⁻¹ K⁻¹ at 773 K). Such prominent low thermal conductivity suggests that the TE performance of our SnSe could be further improved by doping with different elements, such as Na, Te, Ge, Ga, or Cd. ^{3,15,17-19} Given the κ_L remains at the same level, doping could optimize the carrier concentration to overcome the low σ of the derived SnSe. Studies are underway in our laboratories to realize this approach.

The best reported n-type PbSe bulk material has a maximum $ZT \approx 1.5$ (673 K) for Cu/Te co-doped sample, while $ZT \approx 0.8$ (673 K) was reported for n-type Sb-doped PbSe bulk material. The efficiency of our solution-processed undoped n-type PbSe (ZT = 0.73) is on par with that of bulk Sb-doped PbSe and exceeds any reported performance of solution-produced n-type PbSe. The high efficiency obtained for our SPSed PbSe can be related to the tetrapod-like morphology of PbSe building block particles (Figures 3b, S3c,d), thus affording the creation of fine interlocked nano/micro-structure within the resultant SPSed TE material (Figures 3e, S10b). Importantly, to the best of our knowledge, the obtained ZT = 0.73 at 673 K is the highest reported value for any

doped or undoped solution-processed PbSe materials (Figures 8d, 10), albeit the literature on solution-produced thermoelectric PbSe is quite scarce. Cadavid and co-workers reported $ZT \approx 0.6$ at 600 K for colloidal n-type PbSe particles of few nanometers after densification by hot-pressing. Despite high PF = 1.1 mW cm⁻¹ K⁻² and high carrier concentration value of 2.2×10^{19} cm⁻³ at RT, the thermal conductivity and Seebeck coefficient values were reported to be lower than those observed by us.¹² The achieved high efficiency for our solution-processed n-type PbSe further motivates investigating the doping-assisted optimization of carrier concentration in such system.

5. CONCLUSIONS

The preparation of thermoelectric chalcogenides by colloidal synthesis method was successfully developed and afforded ca. 4.5 g of the phase-pure, highly crystalline and defect free PbTe, PbSe, and SnSe particles exhibiting peculiar cube, tetrapod and rod appearances, respectively. Facile synthesis, inexpensive reagents, high yield and upscaling are striking positive points for future application towards chalcogenide preparation.

SPS-assisted sintering of the colloidal synthesis products allowed for the preparation of the phase-pure and high-density PbTe, PbSe, and SnSe pellets with developed fine nano/micro-structure. As a result, the materials demonstrated low thermal conductivity, with a very low value of $\kappa = 0.31 \text{ W m}^{-1} \text{ K}^{-1}$ at 673 K measured for the SPSed SnSe. As thermoelectric materials, *n*-type PbTe and PbSe, as well as *p*-type SnSe demonstrated maximum *ZT* values of 0.31 (623 K), 0.73 (673 K) and 0.34 (673 K), respectively. Studies to improve the modest TE efficiencies of the materials through enhancing their electrical conductivity by means of doping/compositing are currently underway.

ASSOCIATED CONTENT

The Supporting Information is available free of charge at

Details of Hall measurements, as well as additional EDX spectra, SEM images, HAADF-STEM images, STEM-EDX elemental maps, TGA/DSC profiles, and ED patterns (PDF).

AUTHOR INFORMATION

Corresponding Author

Yury V. Kolen'ko – Nanochemistry Research Group, International Iberian Nanotechnology Laboratory, Braga 4715-330, Portugal; orcid.org/0000-0001-7493-1762; Email: yury.kolenko@inl.int

Authors

Viviana Sousa – Center of Physics of the Universities of Minho and Porto, University of Minho,

Braga 4710-057, Portugal; Nanochemistry Research Group, International Iberian

Nanotechnology Laboratory, Braga 4715-330, Portugal

Arka Sarkar – Department of Chemistry, Iowa State University, Ames, Iowa 50011, United States; Ames National Laboratory, U.S. Department of Energy, Ames, Iowa 50011, United States

Oleg I. Lebedev – Laboratoire CRISMAT, UMR 6508, CNRS-ENSICAEN, Caen 14050, France

Christophe Candolfi – Institut Jean Lamour, UMR 7198 CNRS-Université de Lorraine, 2 Allée

André Guinier-Campus ARTEM, BP 50840, CEDEX, Nancy 54011, France

Bertrand Lenoir – Institut Jean Lamour, UMR 7198 CNRS-Université de Lorraine, 2 Allée André Guinier-Campus ARTEM, BP 50840, CEDEX, Nancy 54011, France

Rodrigo Coelho – Centro de Ciências e Tecnologias Nucleares (C2TN), Departamento de Engenharia e Ciências Nucleares, Instituto Superior Técnico, Universidade de Lisboa, Estrada Nacional 10, Bobadela LRS 2695-066, Portugal

António P. Gonçalves – Centro de Ciências e Tecnologias Nucleares (C2TN), Departamento de Engenharia e Ciências Nucleares, Instituto Superior Técnico, Universidade de Lisboa, Estrada Nacional 10, Bobadela LRS 2695-066, Portugal

Eliana M. F. Vieira – CMEMS – UMinho, University of Minho, Guimarães 4800-058, Portugal; LABBELS – Associate Laboratory, Braga, Guimarães, Portugal

Pedro Alpuim – Center of Physics of the Universities of Minho and Porto, University of Minho, Braga 4710-057, Portugal; International Iberian Nanotechnology Laboratory, Braga 4715-330, Portugal

Kirill Kovnir – Department of Chemistry, Iowa State University, Ames, Iowa 50011, United States; Ames National Laboratory, U.S. Department of Energy, Ames, Iowa 50011, United States

Notes

The authors declare no competing financial interests.

ACKNOWLEDGMENTS

This research was supported by Portuguese Fundação para a Ciência e a Tecnologia (FCT) through Contracts UID/Multi/04349/2020 and UI/BD/150713/2020. V.S. acknowledges support by the FCT PhD Fellowship (Grant No. SFRH/BD/143750/2019). E.M.F.V. thanks CMEMS-UMinho Strategic Projects UIDB/04436/2020 and UIDP/04436/2020. The authors are grateful to Prof. J.V. Zaikina (Iowa State University) for access to the SPS instrument. A.S. and K.K. acknowledge support from the National Science Foundation grant DMR-2003783. PPMS instrument used for Hall measurements was supported by Ames National Laboratory, U.S. Department of Energy, which operates under Contract DE-AC02-07CH11358.

REFERENCES

- (1) He, J.; Tritt, M. T. Advances in Thermoelectric Materials Research: Looking Back and Moving Forward. *Science* (80-.). **2017**, 357, eaak9997. https://doi.org/10.1126/science.aak9997.
- (2) Yan, Q.; Kanatzidis, M. G. High-Performance Thermoelectrics and Challenges for Practical Devices. *Nat. Mater* **2021**, *21*, 503–513. https://doi.org/10.1038/s41563-021-01109-w.
- Zhou, C.; Lee, Y. K.; Yu, Y.; Byun, S.; Luo, Z.-Z.; Lee, H.; Ge, B.; Lee, Y.-L.; Chen, X.; Lee, J. Y.; Cojocaru-Mirédin, O.; Chang, H.; Im, J.; Cho, S.-P.; Wuttig, M.; Dravid, V. P.; Kanatzidis, M. G.; Chung, I. Polycrystalline SnSe with a Thermoelectric Figure of Merit Greater than the Single Crystal. *Nat. Mater.* 2021, 20, 1378–1384. https://doi.org/10.1038/s41563-021-01064-6.
- (4) Neophytou, N.; Foster, S.; Vargiamidis, V.; Pennelli, G.; Narducci, D. Nanostructured Potential Well/Barrier Engineering for Realizing Unprecedentedly Large Thermoelectric Power Factors. *Mater. Today Phys.* **2019**, *11*, 100159. https://doi.org/10.1016/j.mtphys.2019.100159.
- (5) Hong, M.; Chasapis, T. C.; Chen, Z.-G.; Yang, L.; Kanatzidis, M. G.; Snyder, G. J.; Zou, J. *N*-Type Bi₂Te_{3-x}Se_x Nanoplates with Enhanced Thermoelectric Efficiency Driven by Wide-Frequency Phonon Scatterings and Synergistic Carrier Scatterings. *ACS Nano* **2016**, *10*, 4719–4727. https://doi.org/10.1021/acsnano.6b01156.
- (6) Zhou, C.; Lee, Y. K.; Cha, J.; Yoo, B.; Cho, S. P.; Hyeon, T.; Chung, I. Defect Engineering for High-Performance *n*-Type PbSe Thermoelectrics. *J. Am. Chem. Soc.* **2018**, *140*, 9282–9290. https://doi.org/10.1021/jacs.8b05741.

- (7) Dresselhaus, M. S.; Chen, G.; Tang, M. Y.; Yang, R.; Lee, H.; Wang, D.; Ren, Z.; Fleurial, J.-P.; Gogna, P. New Directions for Low-Dimensional Thermoelectric Materials. *Adv. Mater.* **2007**, *19* (8), 1043–1053. https://doi.org/10.1002/adma.200600527.
- (8) Lee, M. H.; Yun, J. H.; Kim, G.; Lee, J. E.; Park, S.-D.; Reith, H.; Schierning, G.; Nielsch, K.; Ko, W.; Li, A.-P.; Rhyee, J.-S. Synergetic Enhancement of Thermoelectric Performance by Selective Charge Anderson Localization-Delocalization Transition in *n*-Type Bi-Doped PbTe/Ag2Te Nanocomposite. *ACS Nano* 2019, 13, 3806–3815. https://doi.org/10.1021/acsnano.8b08579.
- (9) Yang, L.; Chen, Z. G.; Hong, M.; Wang, L.; Kong, D.; Huang, L.; Han, G.; Zou, Y.; Dargusch, M.; Zou, J. N-Type Bi-Doped PbTe Nanocubes with Enhanced Thermoelectric Performance. Nano Energy 2017, 31, 105–112. https://doi.org/10.1016/j.nanoen.2016.11.027.
- (10) Fang, H.; Feng, T.; Yang, H.; Ruan, X.; Wu, Y. Synthesis and Thermoelectric Properties of Compositional-Modulated Lead Telluride-Bismuth Telluride Nanowire Heterostructures.

 Nano Lett. 2013, 13, 2058–2063. https://doi.org/10.1021/nl400319u.
- (11) Wang, R. Y.; Feser, J. P.; Lee, J. S.; Talapin, D. V.; Segalman, R.; Majumdar, A. Enhanced Thermopower in PbSe Nanocrystal Quantum Dot Superlattices. *Nano Lett.* **2008**, *8*, 2283–2288. https://doi.org/10.1021/nl8009704.
- Cadavid, D.; Ortega, S.; Illera, S.; Liu, Y.; Ibáñez, M.; Shavel, A.; Zhang, Y.; Li, M.; López,
 A. M.; Noriega, G.; Durá, O. J.; López De La Torre, M. A.; Prades, J. D.; Cabot, A.
 Influence of the Ligand Stripping on the Transport Properties of Nanoparticle-Based PbSe
 Nanomaterials. ACS Appl. Energy Mater. 2020, 3, 2120–2129.

- https://doi.org/10.1021/acsaem.9b02137.
- (13) Zhou, N.-N.; Hu, Z. Q.; Nasser, R.; Song, J. M. Thermoelectric Properties of PbSe Nanocomposites from Solution-Processed Building Blocks. ACS Appl. Energy Mater. 2021, 4, 2014–2019. https://doi.org/10.1021/acsaem.0c03255.
- (14) Zhou, C.; Yu, Y.; Lee, Y. K.; Cojocaru-Mirédin, O.; Yoo, B.; Cho, S. P.; Im, J.; Wuttig, M.; Hyeon, T.; Chung, I. High-Performance *n*-Type PbSe-Cu2Se Thermoelectrics through Conduction Band Engineering and Phonon Softening. *J. Am. Chem. Soc.* 2018, *140*, 15535–15545. https://doi.org/10.1021/jacs.8b10448.
- (15) Lou, X.; Li, S.; Chen, X.; Zhang, Q.; Deng, H.; Zhang, J.; Li, D.; Zhang, X.; Zhang, Y.; Zeng, H.; Tang, G. Lattice Strain Leads to High Thermoelectric Performance in Polycrystalline SnSe. ACS Nano 2021, 15, 8204–8215. https://doi.org/10.1021/acsnano.1c01469.
- (16) Liu, Y.; Calcabrini, M.; Yu, Y.; Lee, S.; Chang, C.; David, J.; Ghosh, T.; Spadaro, M. C.; Xie, C.; Cojocaru-Mirédin, O.; Arbiol, J.; Ibáñez, M. Defect Engineering in Solution-Processed Polycrystalline SnSe Leads to High Thermoelectric Performance. ACS Nano 2022, 16, 78–88. https://doi.org/10.1021/acsnano.1c06720.
- (17) Chandra, S.; Biswas, K. Realization of High Thermoelectric Figure of Merit in Solution Synthesized 2D SnSe Nanoplates via Ge Alloying. *J. Am. Chem. Soc.* **2019**, *141*, 6141–6145. https://doi.org/10.1021/jacs.9b01396.
- (18) Shi, X.; Wu, A.; Feng, T.; Zheng, K.; Liu, W.; Sun, Q.; Hong, M.; Pantelides, S. T.; Chen, Z. G.; Zou, J. High Thermoelectric Performance in *p*-Type Polycrystalline Cd-Doped SnSe

- Achieved by a Combination of Cation Vacancies and Localized Lattice Engineering. *Adv. Energy Mater.* **2019**, 1803242. https://doi.org/10.1002/aenm.201803242.
- (19) Zhang, Y.; Liu, Y.; Xing, C.; Xing, C.; Zhang, T.; Li, M.; Pacios, M.; Yu, X.; Arbiol, J.; Arbiol, J.; Llorca, J.; Cadavid, D.; Ibáñez, M.; Cabot, A.; Cabot, A. Tin Selenide Molecular Precursor for the Solution Processing of Thermoelectric Materials and Devices. ACS Appl. Mater. Interfaces 2020, 12, 27104–27111. https://doi.org/10.1021/acsami.0c04331.
- (20) De Roo, J. Chemical Considerations for Colloidal Nanocrystal Synthesis. *Chem. Mater.* 2022, 34, 5766–5779. https://doi.org/10.1021/acs.chemmater.2c01058.
- (21) Sun, Y.; Terrones, M.; Schaak, R. E. Colloidal Nanostructures of Transition-Metal Dichalcogenides. *Acc. Chem. Res.* **2021**, *54*, 1517–1527. https://doi.org/10.1021/acs.accounts.1c00006.
- (22) Piotrowski, M.; Franco, M.; Sousa, V.; Rodrigues, J.; Deepak, F. L.; Kakefuda, Y.; Kawamoto, N.; Baba, T.; Owens-Baird, B.; Alpuim, P.; Kovnir, K.; Mori, T.; Kolen'Ko, Y. V. Probing of Thermal Transport in 50 Nm Thick PbTe Nanocrystal Films by Time-Domain Thermoreflectance. *J. Phys. Chem. C* 2018, 122, 27127–27134. https://doi.org/10.1021/acs.jpcc.8b04104.
- (23) Piotrowski, M.; Borme, J.; Carbó-Argibay, E.; Sharma, D.; Nicoara, N.; Sadewasser, S.; Petrovykh, D. Y.; Rodríguez-Abreu, C.; Kolen'Ko, Y. V. Template-Directed Self-Organization of Colloidal PbTe Nanocrystals into Pillars, Conformal Coatings, and Self-Supported Membranes. *Nanoscale Adv.* 2019, 1, 3049. https://doi.org/10.1039/c9na00370c.
- (24) Sousa, V.; Savelli, G.; Lebedev, O. I.; Kovnir, K.; Correia, J. H.; Vieira, E. M. F.; Alpuim,

- P.; Kolen'ko, Y. V. High Seebeck Coefficient from Screen-Printed Colloidal PbSe Nanocrystals Thin Film. *Materials (Basel)*. **2022**, *15*, 8805. https://doi.org/https://doi.org/10.3390/ma15248805.
- (25) Sousa, V.; Gonçalves, B. F.; Franco, M.; Ziouani, Y.; González-Ballesteros, N.; Cerqueira, M. F.; Yannello, V.; Kovnir, K.; Lebedev, O. I.; Kolen'Ko, Y. V. Superstructural Ordering in Hexagonal CuInSe₂ Nanoparticles. *Chem. Mater.* 2019, 31, 260–267. https://doi.org/10.1021/acs.chemmater.8b04368.
- (26) Chauhan, N. S.; Lebedev, O. I.; Kovnir, K.; Pyrlin, S. V.; Marques, L. S. A.; Ramos, M. M. D.; Korgel, B. A.; Kolen'Ko, Y. V. Scalable Colloidal Synthesis of Bi2Te2.7Se0.3 Plate-like Particles Give Access to a High-Performing *n*-Type Thermoelectric Material for Low Temperature Application. *Nanoscale Adv.* 2020, 2, 5699. https://doi.org/10.1039/d0na00691b.
- (27) Chauhan, N. S.; Pyrlin, S. V.; Lebedev, O. I.; Marques, L. S. A.; Ramos, M. M. D.; Maiti, T.; Kovnir, K.; Korgel, B. A.; Kolen'Ko, Y. V. Compositional Fluctuations Mediated by Excess Tellurium in Bismuth Antimony Telluride Nanocomposites Yield High Thermoelectric Performance. *J. Phys. Chem. C* 2021, 125, 20184–20194. https://doi.org/10.1021/acs.jpcc.1c05375.
- (28) Zhong, Y.; Tang, J.; Liu, H.; Chen, Z.; Lin, L.; Ren, D.; Liu, B.; Ang, R. Optimized Strategies for Advancing *n*-Type PbTe Thermoelectrics: A Review. *ACS Appl. Mater. Interfaces* **2020**, *12*, 49323–49334. https://doi.org/10.1021/acsami.0c15730.
- (29) Jia, B. H.; Jiang, B. B.; He, J. Q. Recent Advances of *n*-Type Low-Cost PbSe-Based Thermoelectric Materials. *Mater. Today Adv.* **2019**, *4*, 100029.

- https://doi.org/10.1016/j.mtadv.2019.100029.
- (30) Kim, H. S.; Gibbs, Z. M.; Tang, Y.; Wang, H.; Snyder, G. J. Characterization of Lorenz Number with Seebeck Coefficient Measurement. *APL Mater.* **2015**, *3*, 041506. https://doi.org/10.1063/1.4908244.
- (31) Borup, K. A.; Toberer, E. S.; Zoltan, L. D.; Nakatsukasa, G.; Errico, M.; Fleurial, J. P.; Iversen, B. B.; Snyder, G. J. Measurement of the Electrical Resistivity and Hall Coefficient at High Temperatures. *Rev. Sci. Instrum.* **2012**, 83, 123902. https://doi.org/10.1063/1.4770124.
- (32) Chen, Z.; Ge, B.; Li, W.; Lin, S.; Shen, J.; Chang, Y.; Hanus, R.; Snyder, G. J.; Pei, Y. Vacancy-Induced Dislocations within Grains for High-Performance PbSe Thermoelectrics.

 Nat. Commun. 2017, 8, 13828. https://doi.org/10.1038/ncomms13828.
- (33) Kim, S. Il; Lee, K. H.; Mun, H. A.; Kim, H. S.; Hwang, S. W.; Roh, J. W.; Yang, D. J.; Shin, W. H.; Li, X. S.; Lee, Y. H.; Snyder, G. J.; Kim, S. W. Dense Dislocation Arrays Embedded in Grain Boundaries for High-Performance Bulk Thermoelectrics. *Science* (80-.). 2015, 348, 109–114. https://doi.org/10.1126/science.aaa4166.
- (34) Wang, H.; Schechtel, E.; Pei, Y.; Snyder, G. J. High Thermoelectric Efficiency of *n*-Type PbS. *Adv. Energy Mater.* **2013**, *3*, 488–495. https://doi.org/10.1002/aenm.201200683.
- (35) Zhou, C.; Yu, Y.; Lee, Y. L.; Ge, B.; Lu, W.; Cojocaru-Mirédin, O.; Im, J.; Cho, S. P.; Wuttig, M.; Shi, Z.; Chung, I. Exceptionally High Average Power Factor and Thermoelectric Figure of Merit in *n*-Type PbSe by the Dual Incorporation of Cu and Te. *J. Am. Chem. Soc.* 2020, *142*, 15172–15186. https://doi.org/10.1021/jacs.0c07712.

- (36) Shi, X.-L.; Chen, W.-Y.; Tao, X.; Zou, J.; Chen, Z.-G. Rational Structural Design and Manipulation Advance SnSe Thermoelectrics. *Mater. Horiz.* **2020**, *7*, 3065–3096. https://doi.org/10.1039/d0mh00954g.
- (37) Goldsmid, H. J.; Sharp, J. W. Estimation of the Thermal Band Gap of a Semiconductor from Seebeck Measurements. *J. Electron. Mater.* **1999**, *28*, 869–872. https://doi.org/10.1007/s11664-999-0211-y.
- (38) Xiao, Y.; Zhao, L.-D. Charge and Phonon Transport in PbTe-Based Thermoelectric Materials. *npj Quantum Mater.* **2018**, *3*, 55. https://doi.org/10.1038/s41535-018-0127-y.
- Zhao, L.-D.; Lo, S.-H.; Zhang, Y.; Sun, H.; Tan, G.; Uher, C.; Wolverton, C.; Dravid, V.
 P.; Kanatzidis, M. G. Ultralow Thermal Conductivity and High Thermoelectric Figure of
 Merit in SnSe Crystals. *Nature* 2014, 508, 373–377. https://doi.org/10.1038/nature13184.
- (40) Wang, H.; Pei, Y.; LaLonde, A. D.; Snyder, G. J. Weak Electron-Phonon Coupling Contributing to High Thermoelectric Performance in *n*-Type PbSe. *Proc. Natl. Acad. Sci. U.S.A.* **2012**, *109*, 9705–9709. https://doi.org/10.1073/pnas.1111419109.
- (41) Xu, F.; Zhang, D.; Gao, S.; Yang, L.; San, X.; Li, Z.; Qian, X.; Yang, J.; Wang, S. Effects of La Doping Induced Carrier Concentration Regulation and Band Structure Modification on Thermoelectric Properties of PbSe. Scr. Mater. 2022, 208, 114360. https://doi.org/10.1016/j.scriptamat.2021.114360.
- Zhang, Q.; Chere, E. K.; McEnaney, K.; Yao, M.; Cao, F.; Ni, Y.; Chen, S.; Opeil, C.; Chen,
 G.; Ren, Z. Enhancement of Thermoelectric Performance of *n*-Type PbSe by Cr Doping with Optimized Carrier Concentration. *Adv. Energy Mater.* 2015, 5, 1401977.

- https://doi.org/10.1002/aenm.201401977.
- (43) Gayner, C.; Kar, K. K.; Kim, W. Recent Progress and Futuristic Development of PbSe Thermoelectric Materials and Devices. *Mater. Today Energy* **2018**, *9*, 359–376. https://doi.org/10.1016/j.mtener.2018.06.010.
- (44) Vineis, C. J.; Harman, T. C.; Calawa, S. D.; Walsh, M. P.; Reeder, R. E.; Singh, R.; Shakouri, A. Carrier Concentration and Temperature Dependence of the Electronic Transport Properties of Epitaxial PbTe and PbTe/PbSe Nanodot Superlattices. *Phys. Rev. B Condens. Matter* 2008, 77, 235202. https://doi.org/10.1103/PhysRevB.77.235202.
- (45) Wang, X.; Wu, G.; Cai, J.; Zhang, Q.; Yang, J.; Chen, L.; Hu, H.; Liu, G.; Tan, X.; Jiang, J. Unusually High Seebeck Coefficient Arising from Temperature-Dependent Carrier Concentration in PbSe-AgSbSe₂ Alloys. *J. Mater. Chem. C* 2021, 9, 17365. https://doi.org/10.1039/d1tc04158d.
- (46) Sun, J.; Zhang, Y.; Fan, Y.; Tang, X.; Tan, G. Strategies for Boosting Thermoelectric Performance of PbSe: A Review. *Chem. Eng. J.* **2022**, *431*, 133699. https://doi.org/10.1016/j.cej.2021.133699.
- (47) Wang, X.; Li, X.; Zhang, Z.; Chen, C.; Li, S.; Lin, X.; Sui, J.; Liu, X.; Cao, F.; Yang, J.; Zhang, Q. Thermoelectric Properties of *n*-Type Transition Metal-Doped PbSe. *Mater. Today Phys.* **2018**, *6*, 45–52. https://doi.org/10.1016/j.mtphys.2018.06.004.
- (48) Vaqueiro, P. Chapter 1. Synthesis and Property Measurements of Thermoelectric Materials; 2021. https://doi.org/10.1039/9781788019590-00001.
- (49) Zhang, Q.; Wang, H.; Liu, W.; Wang, H.; Yu, B.; Zhang, Q.; Tian, Z.; Ni, G.; Lee, S.;

Esfarjani, K.; Chen, G.; Ren, Z. Enhancement of Thermoelectric Figure-of-Merit by Resonant States of Aluminium Doping in Lead Selenide. *Energy Environ. Sci.* **2012**, *5*, 5246. https://doi.org/10.1039/c1ee02465e.

